Analysis of crack propagation behavior in concrete due to multi-rebar corrosion

Khoa K. TRAN[1], Hikaru NAKAMURA[2], Minoru KUNIEDA[3] and Naoshi UEDA[4]

[1] Doctoral student, Dept. of Civil Eng., Nagoya University
(Furo-cho, Chikusa-ku, Nagoya, 464-8601, Japan)
E-mail:tk.khoa@gmail.com

[2]Member of JSCE, Professor, Dept. of Civil Eng., Nagoya University
(Furo-cho, Chikusa-ku, Nagoya, 464-8601, Japan)
E-mail: hikaru@civil.nagoya-u.ac.jp

[3]Member of JSCE, Associate Professor, Dept. of Civil Eng., Nagoya University
(Furo-cho, Chikusa-ku, Nagoya, 464-8601, Japan)
E-mail: kunieda@civil.nagoya-u.ac.jp

[3]Member of JSCE, Assistant Professor, Dept. of Civil Eng., Nagoya University
(Furo-cho, Chikusa-ku, Nagoya, 464-8601, Japan)
E-mail: ueda@civil.nagoya-u.ac.jp

Analytical model developed by the authors, using three-dimensional Rigid-Body-Spring-Method (RBSM) combined with a three-phase material corrosion-expansion model, was verified against experiments in the case of multi-rebar corrosion. The experiments of beams having multi-rebars were carried out by the other researchers using electric corrosion tests. The applicability of the analytical model was confirmed in terms of crack patterns, surface crack width and internal crack propagation due to multi-rebar corrosion. Moreover, a mechanism of crack propagation in concrete due to multi-rebar corrosion was investigated and compared with the case of single-rebar corrosion analytically. As a result, it was found that rebar spacing strongly affects crack patterns and crack propagation mechanism of concrete. Internal cracks are dominant rather than surface cracks and the propagation of internal cracks combined with surface cracks may cause de-lamination of the concrete cover.

Key Words : *multi-rebar, rigid body spring method, internal crack ,rebar spacing, de-lamination*

1. Introduction

Cracking of concrete due to rebar corrosion is a major deterioration behavior in concrete structures and it accelerates deterioration as well as causes de-lamination of the concrete cover. Therefore, the study to clarify cracking behavior due to rebar corrosion has been done by many researchers[1,2].

Cracking propagation resulting from rebar corrosion in the case of single rebar specimens have been clarified experimentally and analytically. For example, Tsutsumi et al (1995) clarified the cracking patterns depending on ratio of cover thickness and rebar diameter of the single rebar corrosion experimentally[3], which is, if the concrete cover is thick, cracks propagate from rebar to concrete surface in the shortest path and to horizontal direction, and if the concrete cover is thin, cracks develop diagonally to concrete surface and cause a spalling of concrete cover. In the analytical study, finite element method have been usually performed in which corrosion expansion model is combined to simulate cracking propagation due to rebar corrosion[4].

The authors have also analyzed the crack propagation of the single rebar corrosion specimens, in which the RBSM analytical model combined with the three-phase material corrosion expansion model was developed to evaluate crack propagation behavior[5]. Properties of corrosion products such as initial thickness and elastic modulus were recommended for the analytical model. Some effects on crack propagation such as local corrosion models and penetration of corrosion products into cracks were clarified analytically. The analytical results were qualitatively and quantitatively confirmed with the testing results such as crack patterns, internal crack length and crack width.

Several researchers carried out experiment of multi-rebar specimens using electric corrosion tests to evaluate cracking propagation such as crack patterns and crack widths[6,7] , in which internal cracks join together between rebars due to multi rebar arrangement. Some analytical models using finite element method have also been proposed to simulate crack pattern and crack width in the case of

multi-rebar corrosion[7], in which internal cracks significantly develop inside concrete in the case of multi-rebar corrosion. However, a crack propagation mechanism and effects on cracking propagation due to multi-rebar corrosion have not been clarified in the available literature.

In this study, the analytical model developed by the authors was confirmed against experiments of multi-rebar corrosion specimens carried out by other researchers using electric corrosion tests[6,7]. The analytical model shows its applicability to simulate crack propagation of multi-rebar corrosion specimens in terms of crack patterns, surface crack and internal crack propagation. Additionally, an analytical parameter study was carried out for multi-rebar corrosion specimens with varied rebar spacing to investigate effect of rebar spacing on crack patterns, crack propagation, crack joining and surface deformation of concrete cover.

2. Analytical method

The discrete method using Rigid-Body- Spring-Method (RBSM) combined with the three-phase material corrosion model was developed by the authors[5]. The main contents of the analytical development are briefly described as follows.

2.1. Three- dimensional RBSM

The RBSM developed by Kawai employs the discrete numerical analysis method[8]. Analyses of concrete or concrete structures using the RBSM were conducted by Bolander and Saito[9], Ueda et al.[10], Nagoya university group[11] and Nagai et al.[12].

The RBSM represents a continuum material as an assemblage of rigid particle elements interconnected by zero-length springs along their boundaries as shown in Fig. 1. In this study, three-dimensional RBSM is used[13]. Each element has six degrees of freedom at the center points. The boundary between two elements is divided into triangles formed by the center and vertices of the boundary. At each center point of a triangle, three springs- one normal and two shear springs- are set. The analytical model is divided into elements using Voronoi random polygons. In a RBSM model, crack widths can be automatically measured during analysis so it is convenient to directly calculate the volume of cracks in the analysis. It is possible to simulate complicated problems using the three-dimensional RBSM model.

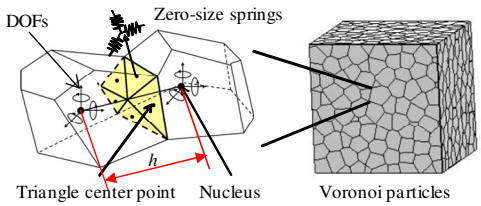

Fig. 1. Voronoi particles definition of RBSM model

2.2. Concrete and rebar material model

Fig. 2 shows the concrete material models that are used in the analysis.

The tensile behavior of concrete up to the tensile strength is modeled as linear elastic. A bilinear softening branch is assumed after cracking as shown, in which f_t is tensile strength, G_F is tensile fracture energy and h is distance between centers of the Voronoi elements.

In the compressive model, the stress-strain relationship is parabolic up to the compressive strength f'_c. The initial stiffness, E, is Young's modulus of concrete. After the peak, the softening branch exists until failure. G_{Fc} is compressive fracture energy and it is calculated as follows[14]:

$$G_{Fc} = 8.8 \cdot \sqrt{f'_c} \qquad (1)$$

Normal springs are set to represent the tensile and compressive properties of concrete. Strain of the normal springs is defined as follows:

$$\varepsilon = \frac{\Delta n}{h} \qquad (2)$$

where ε is strain of the normal springs and Δn is normal relative displacement of elements of those springs.

Tangential (shear) springs represent the shear transferring- mechanism of concrete. Strain of the shear springs is defined as follows:

$$\gamma = \frac{\Delta s}{h} \qquad (3)$$

where γ is strain of the shear springs and Δs is shear relative displacement of elements of those springs.

The shear strength is assumed to follow the Mohr-Coulomb type criterion with the tension and compression caps, in which, c is cohesion and ϕ is internal friction and τ is shear stress. The shear-fracture criterion is expressed as follows[15]:

$$\frac{\tau^2}{\tau_f^2} \geq 1 \qquad (4)$$

where

$$\tau_f = \begin{cases} c - \sigma \tan\phi, & \text{for} \quad \sigma \geq 0.5 f'_c \\ c - 0.5 f'_c \tan\phi, & \text{for} \quad \sigma < 0.5 f'_c \end{cases}$$

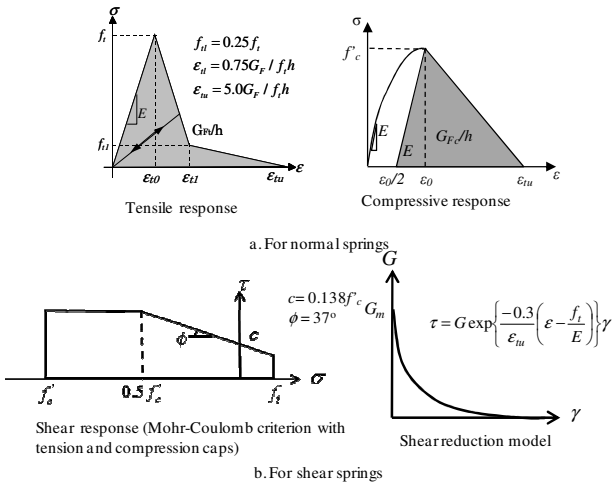

Fig. 2. Concrete material model

After the shear stress reaches the yield strength, the stress moves on the yield surface until the shear strain reaches the ultimate strain γ_u. The force in the shear spring is released and the local stiffness is set to zero when the shear strain exceeds the ultimate strain. The ultimate strain is set to 4000μ in this study.

The shear transferring capacity at the cracked interface changes according to the crack opening. In order to take account of this effect, the shear stiffness is reduced by using a function of the strain normal to the crack as shown in the shear-reduction model in Fig. 2b, in which G is the shear stiffness. Springs set on boundary behave elastically until stresses reach the τ_{max} criterion or the tensile strength f_t [11].

Rebar is modeled as linear elastic in the analysis with the modulus of elasticity being 200 GPa.

The three-dimensional analysis can simulate complex problems[16] such as longitudinal local corrosion along the length of rebar, pitting corrosion along the length of the rebar as well as the spalling behavior of concrete surface due to rebar corrosion. In these cases, a two-dimensional analysis cannot simulate reasonably.

2.3. Corrosion expansion model

In the RBSM analytical model, the expansion of corrosion products is modeled as shown in Fig. 3. A three-phase material model including rebar, corrosion products and concrete is applied. The merit of the model is that the properties of corrosion products such as thickness (H) and elastic modulus (E_r) are directly assumed.

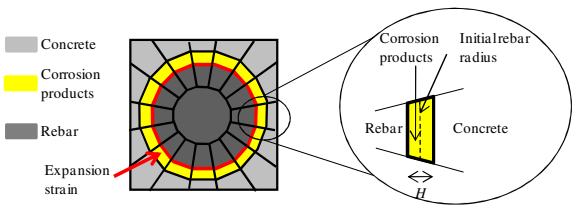

Fig. 3. RBSM corrosion expansion model

The corrosion products layer is modeled by an elastic material model with unloading occurs to the origin. Due to nature of the corrosion process, we assume that internal expansion pressure is only activated in the normal direction, so strain is applied only to the normal springs located on the boundary between the corrosion products layer and the rebar. Strain in the corrosion product layer is determined[17]:

$$\varepsilon_{cor} = \frac{U_{cor} - U}{H} \qquad (5)$$

where U_{cor} is real increase of the rebar radius corresponding to confinement of the concrete and U is free increase of the rebar radius due to rebar corrosion.

On the other hand, shear stiffness of shears springs of the corrosion products layer is set nearly zero in the analysis to simulate free sliding of corrosion products layer in shear direction.

Normal stress distribution in the corrosion products layer is determined based on the linear stress-strain relationship. Increment of a normal stress in the corrosion layer at each analysis step is determined as follows:

$$\Delta\sigma_{cor} = E_r(\Delta\varepsilon - \Delta\varepsilon_0) \qquad (6)$$

in which, $\Delta\varepsilon = \frac{\Delta U_{cor}}{H}$ is increment of total strain and $\Delta\varepsilon_0 = \frac{\Delta U}{H}$ is increment of initial strain.

The internal expansion due to rebar corrosion is simulated using the initial strain problem with increment of initial strain in each analysis step, in which ΔU is an increment of the free increase U and is input data in each analysis step.

In this study, values of corrosion products properties such as layer thickness (H) and elastic modulus (E_r) are 1 mm and 500 MPa respectively as recommended in our previous study[5].

Regarding the distribution of corrosion products on rebar section, the local corrosion HALF model as shown in Fig. 4 is assumed in the analysis as discussed in the previous study[5] and observed in some tests [18].

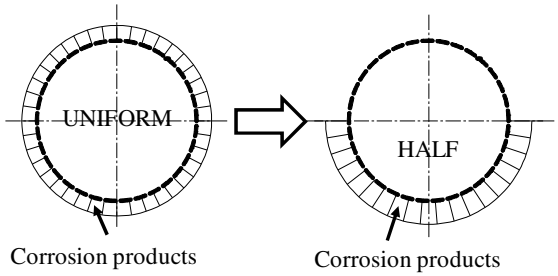

Fig. 4. Local corrosion model

In the previous study[5], the effect of penetration of

corrosion products into cracks was considered. This effect caused the degradation of corrosion products volume after crack initiation and propagation. This effect influenced the propagation of crack width as clarified in the previous study. In this paper, the penetration of corrosion products into cracks is not taken into account because this study focuses on the propagation of crack pattern due to multi-rebar corrosion.

In the analysis, mesh sizes of the Voronoi particles are 5 mm in the cover thickness and 40 mm in the other areas. The another arrangement of the Voronoi particles was tried to confirm the similarity of the analytical results.

3. Verification of analytical model

3.1. Verification of crack patterns

The electric corrosion test results carried out by Murakami et al[6] is used to verify crack patterns and surface crack width in the case of multi-rebar corrosion. Analyzed specimens are series S0 having 3 D16 rebars with the setting dimensions shown in Fig. 5. The external rebars were labeled L,R and the internal one was labeled M in the specimens.

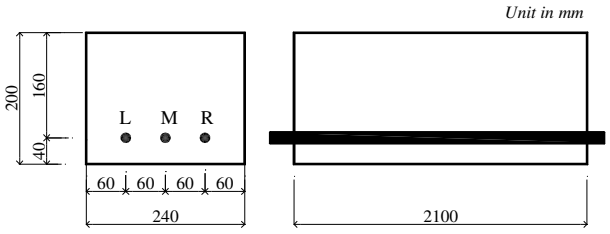

a) Section b) Side view

Fig. 5. Specimens of series S0 (Murakami et al.)

Specimens were tested until average rebar corrosion ratios reached 10.2% (S0-10), 18.6% (S0-20) and 26.4% (S0-30). Before starting the electric corrosion test, the concrete compressive strengths were 31.6, 35.5 and 26.2 MPa corresponding to specimens with rebar corrosion ratios of 10.2%, 18.6% and 26.4%. After finishing the electric corrosion test, crack patterns were observed on the bottom surface of specimens and on the ends of specimens. Surface crack width along the external rebars was also measured for each case of rebar corrosion ratio.

3D-RBSM model of the specimen is shown in Fig. 6. Due to limitation of numerical computation, the specimen's length is modeled as 100 mm in the analysis. Specimens are simply supported on the other side of the concrete cover as shown in Fig. 6c.

Concrete material properties used in the analysis are f'_c=31.0 MPa, f_t=1.92 MPa, E=26.2 GPa and G_F=0.04 N/mm.

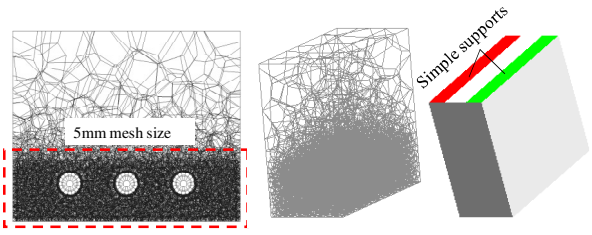

a) Specimen section b) 3D Voronoi particles c) Specimen supports

Fig. 6. RBSM model of specimen S0

Fig. 7 and Fig. 8 shows crack patterns on bottom surface and beam ends in the analysis and the experiment respectively. Analytical surface cracks on bottom surface at rebar corrosion ratio 10.2% (in Fig. 7b) only appear along external rebars over the specimen length which totally agree with the test results shown in Fig. 7a.

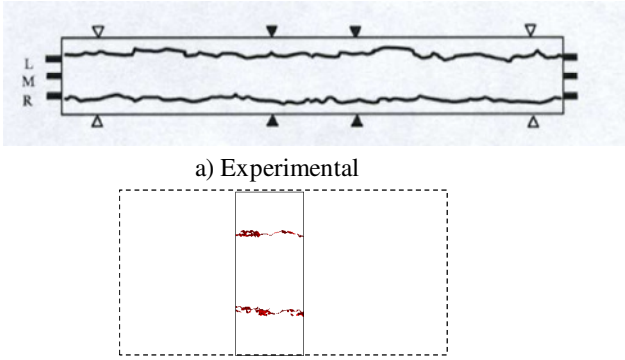

a) Experimental

b) Analytical

Fig. 7. Cracks on bottom surface

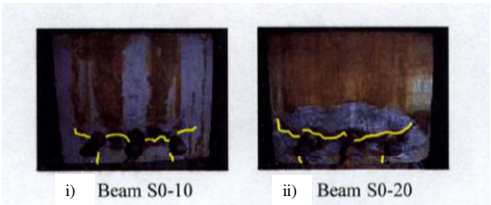

a) Experimental

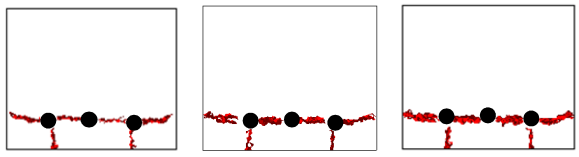

b) Analytical

Fig. 8. Cracks on beam end

On the beam ends, analytical cracks are obtained at rebar corrosion ratios as of 10.2%, 18.6 % and 26.4% and shown in Fig. 8b. There is no crack under M rebar on the concrete cover and cracks between L,R rebars and M rebar are dominant. Internal cracks propagate from the external rebars toward the specimen sides; the internal cracks reach specimen sides when the rebar ratio as 26.4% and they are

longer than the ones when the rebar ratio as 18.6%. Again, the analytical cracks appear agreement with the experimental ones shown in Fig. 8a.

Surface crack width along L, R rebar is also measured in the analysis. The propagation of surface crack against increase of rebar corrosion ratio is shown in Fig. 9. The analytical crack width also agree with the experimental one, in which surface crack width initiates after a particular value of rebar corrosion ratio and then rapidly increase corresponding to increase of corrosion ratio.

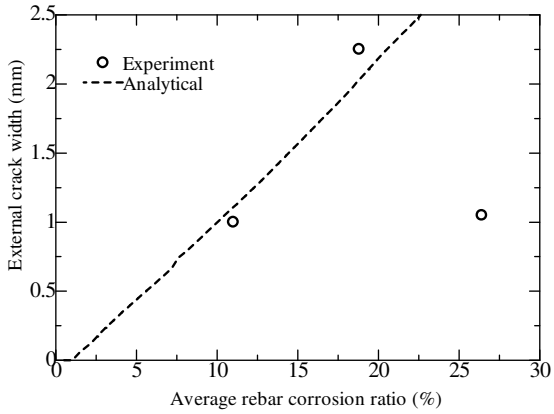

Fig. 9. Surface crack width (along L, R rebar)

3.2. Verification of internal crack propagation

The electric corrosion test results carried out by Admed et al[7] is used to verify propagation of internal crack in the case of multi-rebar corrosion.

In the experiment, internal strain is measured using a 70 mm long concrete embeddable fiber-optic strain sensor (FOSS) as shown in Fig.10.

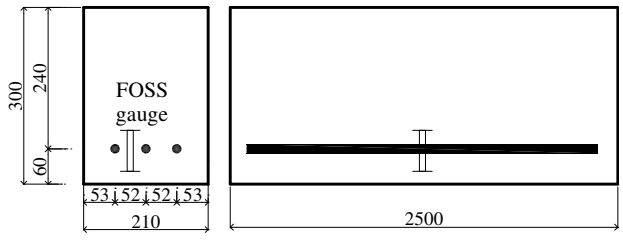

Fig. 10. Specimen dimension and FOSS set-up (Admed et al.)

With this set-up, the FOSS strain is directly proportional to internal crack width between the external rebar and the middle one. The concrete beam having three D16 rebars was accelerated by a corrosion test. The compressive strength of concrete was 40 MPa before the corrosion test.

3D-RBSM model of the specimen and a position to measure internal crack are shown in Fig. 11. Specimen's length is also modeled as 100 mm. Concrete material properties used in the analysis are f'_c=40.0 MPa, f_t=3.35 MPa, E=32.3 GPa and G_F=0.07 N/mm. A merit of RBSM model is that internal crack width can be directly obtained during the analysis.

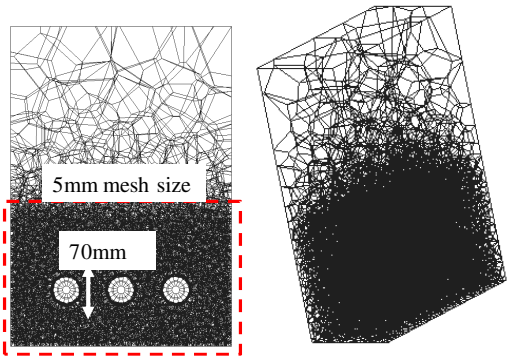

Fig. 11. RBSM model of specimen

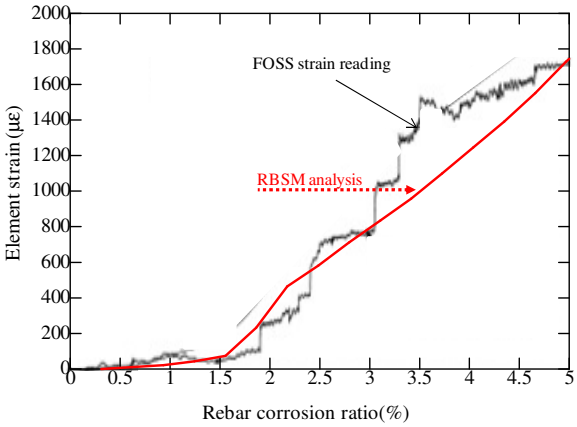

Fig. 12. Analytical internal strain

Fig. 12 shows analytical strain against the experimental FOSS strain gauge's values. The analytical FOSS strain is obtained by dividing the crack width (measured in the analysis) for the distance between the measuring pre-input elements, i.e. 70 mm. So, this is an average value in the analysis which is similar to the measurement way in the experiment. Rebar corrosion ratio is smaller than the results of Murakami's test. The analytical strain shows reasonable agreement with the experimental value, that is internal strain initiates when rebar corrosion ratio around 1.5% and then it speedily propagate when the corrosion ratio increases.

The above verifications prove the applicability of the RBSM analytical model in simulation of crack propagation in the case of multi-rebar corrosion specimens. The applicability is shown qualitatively and quantitatively.

4. Effect of rebar spacing on crack propagation

In this part, a mechanism of crack propagation due to multi-rebar corrosion is discussed.

In order to investigate effect of rebar spacing on crack patterns in the case of multi-rebar corrosion, the specimen in the Murakami's experiment is simulated again with varied rebar spacing dimensions which are varied from 40 mm to 200 mm as shown in Fig. 13. Other dimensions from rebars to specimen surfaces are kept constant to eliminate other effects caused by these factors[19]. Specimen Sr-60 is the same as the specimen series S0.

Moreover, a specimen with single-rebar arranged in the middle of the specimen and the other dimensions are the same with specimen Sr-60 is simulated to compare its behavior with the multi-rebar corrosion specimens.

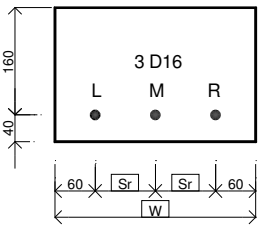

Specimen	Rebar spacing Sr (mm)	Specimen width W(mm)
Sr-40	40	200
Sr-60	60	240
Sr-200	200	520
Single	N/A	240

Fig. 13. Specimens with varied rebar spacing

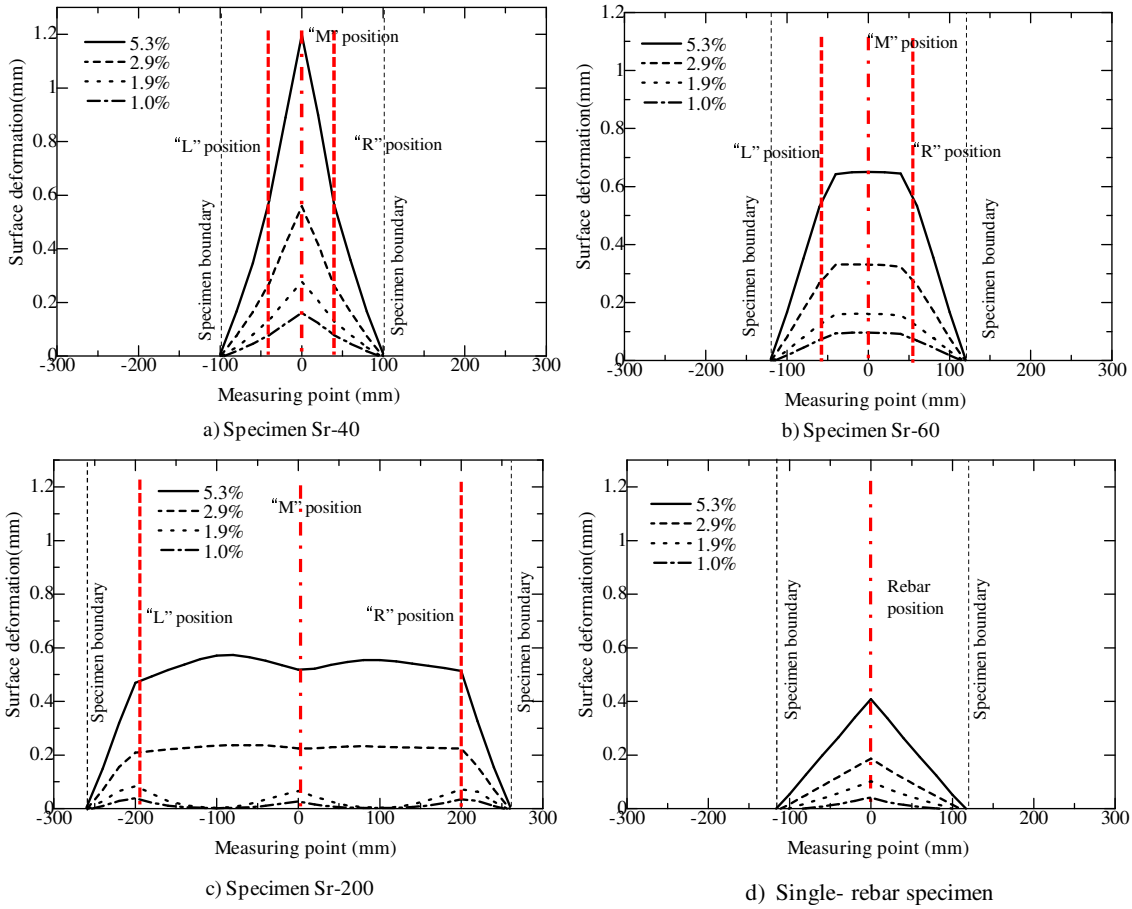

Fig. 14. Surface deformation development

Fig. 14 shows bottom surface deformation of the specimens with varied rebar spacing at several rebar corrosion ratios. In the single rebar specimen, the maximum deformation is at the middle of specimen which is coincide with the rebar position. With the increasing rebar corrosion ratio, deformed area is expanded and the surface deformation is increased. In the multi-rebar corrosion specimens, there are three types of surface deformation shape due to different rebar spacing at corrosion ratio of 1.9%. In specimen Sr-40, the maximum deformation is at the middle of specimen and then it develops with increase of corrosion ratio which is similar to the single-rebar corrosion specimen. In specimen Sr-60, the surface deformation is in a trapezium shape with the changing slope at the L,R rebar position. In specimen Sr-200, initially, surface is bent similar to the single-rebar corrosion case at each rebar position. With further increase of rebar corrosion ratio, surface deformation is increased and changed to a trapezium

shape with the changing slope at the L,R rebar position. Then, the surface deformation increases and changes with a slope reduction at M rebar position. Furthermore, the value of deformation in multi-rebar corrosion specimens is larger than the value of the single-rebar corrosion specimen. It is obviously understood that the crack propagation mechanism of the multi-rebar corrosion specimens is different from the one of the single rebar specimen. Regarding the width of the surface deformed area, in the case of Sr-40, it is noted that the surface deformation width seems to be 200 mm and no change although the rebar corrosion ratio increases. It is due to the propagation of internal cracks reaching the specimen width limitation as shown in this figure, i.e. 200 mm, in the early stage of rebar corrosion. So that, the width of deformed area did not expand more than 200 mm width.

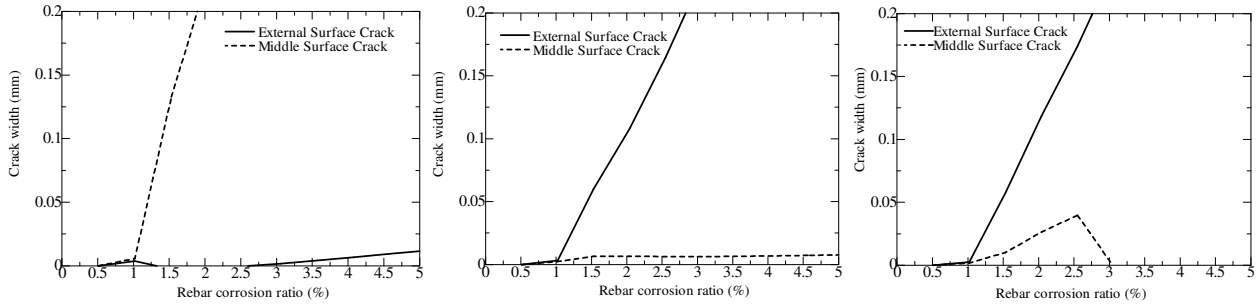

a) Specimen Sr-40 b) Specimen Sr-60 c) Specimen Sr-200

Fig. 15. Propagation of surface crack width (External and Middle)

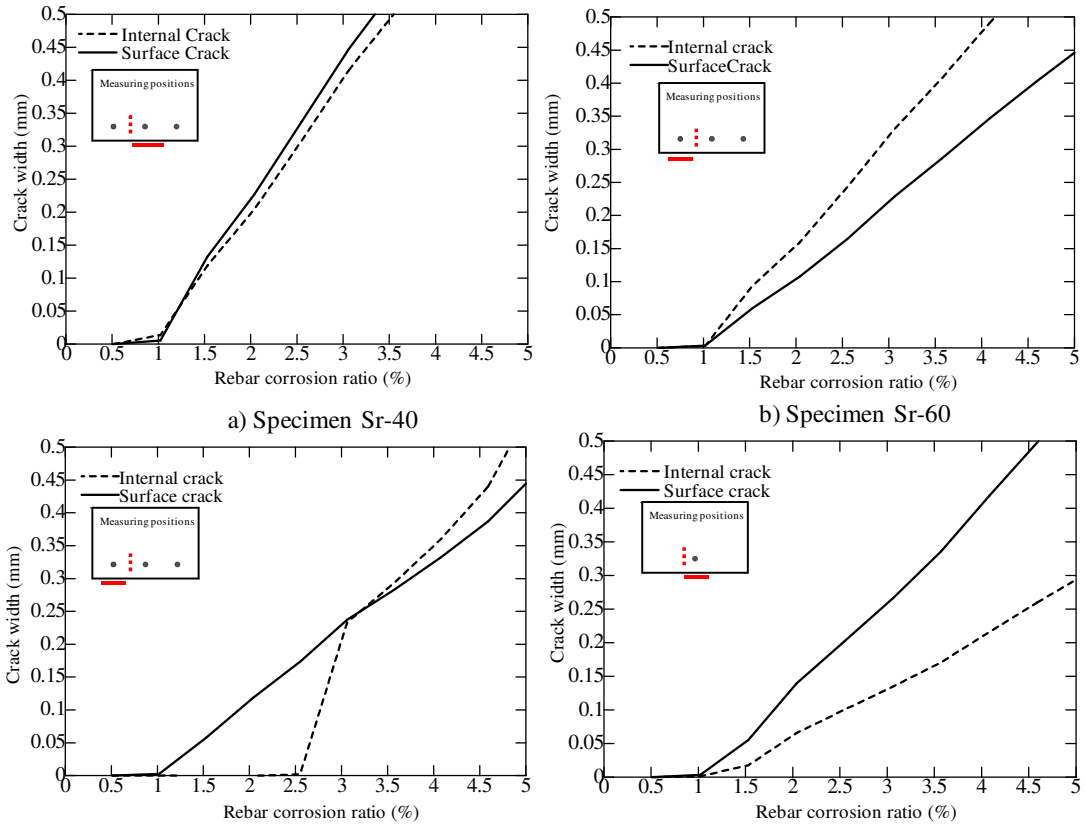

a) Specimen Sr-40 b) Specimen Sr-60

c) Specimen Sr-200 d) Single-rebar specimen

Fig. 16. Propagation of surface crack and internal crack

Fig. 15 shows propagation of surface crack width measured below L,R rebar (external surface cracks) and M rebar (middle surface crack) against increase of rebar corrosion ratio. In specimen Sr-40, the middle surface crack is dominant corresponding to the surface deformation shape. In specimen Sr-60 and specimen Sr-200, external surface crack is dominant. The middle surface crack of Sr-60 increases then keeps its width unchanged after corrosion rebar ratio of 1.5%. The middle surface

crack of Sr-200 rapidly increases after the initiation and then reduces its width at rebar corrosion ratio of 2.5% due to the changing surface deformation at M rebar as shown in Fig. 14. The tendency of specimen Sr-40 is different from the one of Sr- 60 and Sr-200 because due to the closer rebar spacing, specimen Sr-40 behaves similarly to the single-rebar specimen, in which the maximum surface crack opening is at the specimen centre. This behaviour can be understood from the surface deformation shown in Figure 14.a.

Fig. 16 shows propagation of surface crack width and internal crack width against increase of rebar corrosion ratio. Surface crack width is measured below L,R rebar of specimen Sr-60 and Sr-200 and below M rebar of Sr-40 and the single-rebar specimen. Internal crack width is measured between L,R rebar and M rebar in the multi-rebar specimens. In the single-rebar specimen, internal crack width is measured at the position as the same as the one in Sr-60. The diagrams showing crack measuring positions are also added in this figure for clarity. In the single-rebar specimen, surface crack width is larger than internal crack width. On the other hand, in the multi-rebar specimens, internal crack width is basically larger than the surface crack width. In the case of specimen Sr-40, surface crack width and internal crack width are almost the same. In the later stage of specimens Sr-60 and Sr-200, internal crack width is larger than the surface crack width. Surface crack width and internal crack width of specimen Sr-40 are bigger than the ones of specimen Sr-60 and specimen Sr-200. Therefore, in the multi-rebar corrosion cases the propagation of internal cracks should be noted because internal cracks are not easy to observe in the maintenance process.

Fig. 17 represents the indication of crack width in the analysis using stress-crack width relationship. The colors (green, yellow and red) represent crack width values corresponding to the concrete tensile model, in which the range of red color corresponds to large cracks (larger than 0.15 mm width), the yellow one corresponds to 0.02 mm-0.15 mm wide cracks and the green one to minor cracks.

Fig. 18 shows crack development at several rebar corrosion ratios for all specimens. For clarity, the specimens are shown upside down with the rebars on the top side. At rebar corrosion ratio about 0.5%, minor cracks occur around rebars. The minor cracks distribution are similar in specimen Sr-60, Sr-200 and the single-rebar specimen. On the other hand, in Sr-40 specimen, minor cracks join between the rebars and distribute on the surface. The effect of rebar spacing is already observed for narrow rebar spacing case. At rebar corrosion ratio about 1%, internal cracks join together between L,R rebar and M rebar for small rebar spacing specimens (Sr-40, Sr-60). Then, they develop to larger cracks (red color). Surface cracks initiates along L,R rebar in specimen Sr-60 and specimen Sr-200 and along M rebar in specimen Sr-40 corresponding to the bending of surface. This means that internal cracks have already developed when visible surface cracks are observed. In specimen Sr-200, internal cracks become larger after the joining cracks between the rebars at corrosion ratio of 2.5%, the internal cracks are significant dominant in this case rather than surface cracks. In comparison with the single-rebar corrosion, the multi-rebar corrosion causes large internal cracks to be formed earlier, for example, at rebar corrosion ratio of 1.9%, there are significant amount of large cracks (red color) are formed in Sr-40 and Sr-60 rather than the ones of single rebar specimen. This is the effect of multi-rebar arrangement. That is, internal cracks propagate from each rebar to the horizontal direction, internal crack width increases due to the interference of cracks. Therefore, in the single rebar corrosion, the surface crack width is larger than the internal one but in the multi-rebar cases, the internal crack is larger than the surface one.

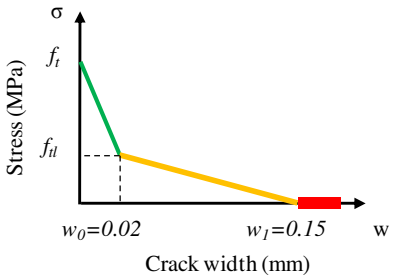

Fig. 17. Indication of crack width

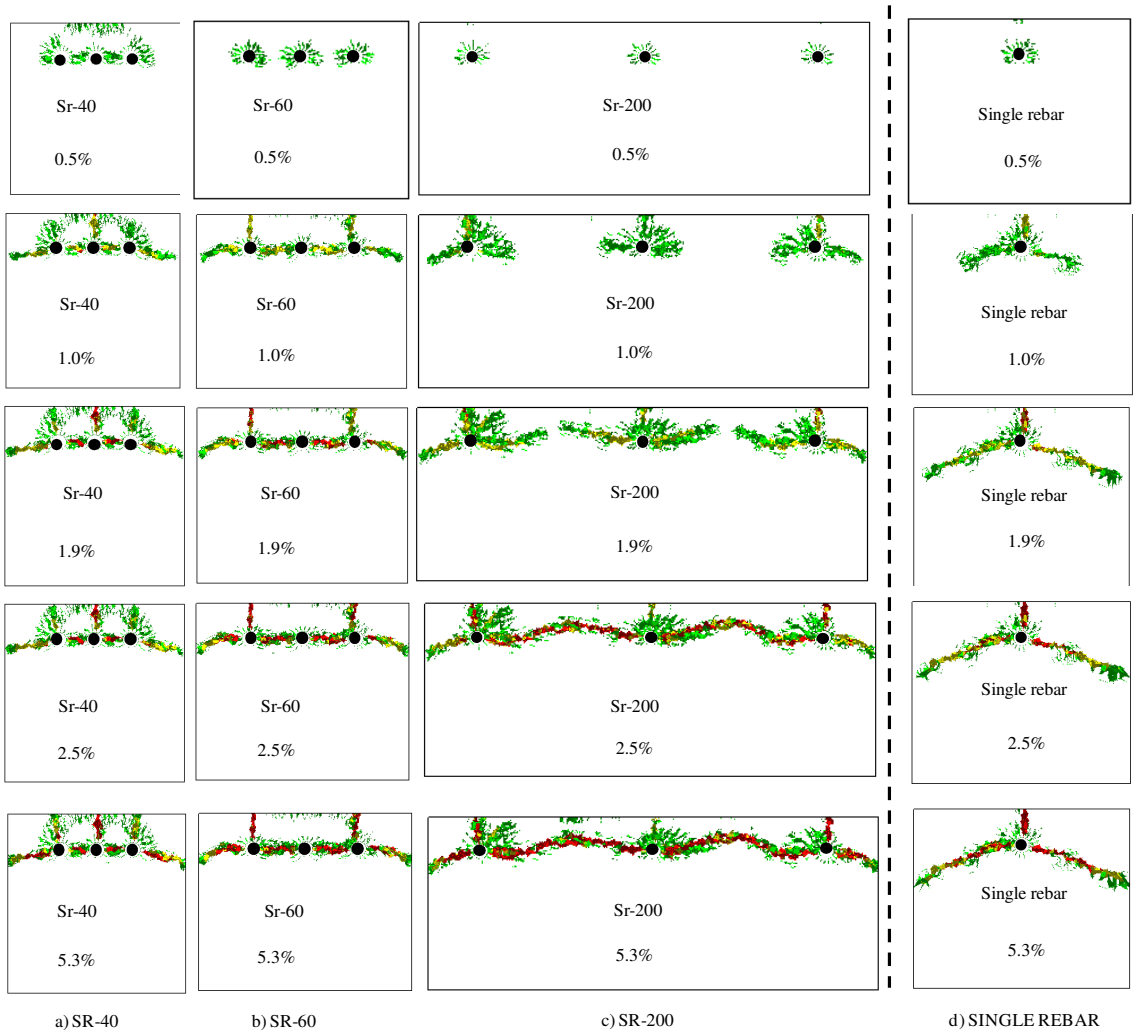

Fig. 18. Crack development

Deformation of specimens at rebar corrosion ratio 5.3% are shown in Fig. 19, in which the specimen are shown upside down. Crack patterns are also understood from the deformation, because the deformation is occurred by the separation between rigid bodies in RBSM. Crack patterns on the beam ends are significantly affected by the rebar spacing. Surface cracks appears along M rebar in specimen Sr-40. Cracks also appears along L,R rebars in specimen Sr-40 but they are not dominant as the one along M rebar. In specimen Sr-60, surface cracks appear along L,R rebar. Surface cracks along M rebar do not propagate. In specimen Sr-200, the surface cracks behave similarly with the ones of specimen Sr-60. In specimens Sr-60 and Sr-200, the middle parts of cover concrete seem to be delaminated due to propagation of internal cracks between rebars and cracks along L, R rebars.

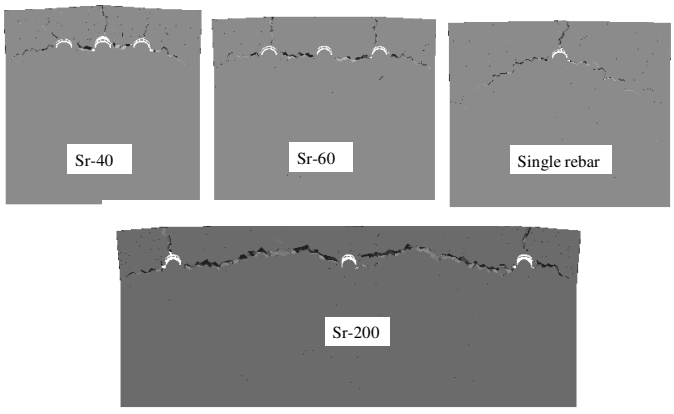

Fig. 19. Specimen deformation at rebar ratio 5.3% (magnification= 5)

5. Conclusion

The purpose of this study is to analyze crack propagation due to multi-rebar corrosion using the 3D-RBSM analytical method, to investigate the effect of rebar spacing on to crack patterns, and to clarify a cracking mechanism of multi-rebar corrosion specimens. The following summary and conclusions were derived from the study.

(1) The applicability of the analytical method was confirmed by the experimental results in terms of crack patterns, surface crack width and internal crack width propagation.
(2) In the case of multi rebar-corrosion, internal cracks joined together between rebars and developed to large cracks earlier than the ones in the single-rebar corrosion.
(3) Rebar spacing significantly affects the crack patterns and crack propagation in the case of the multi-rebar corrosion.
(4) The dominant and the propagation of internal cracks tend to cause de-lamination of the concrete cover in the multi-rebar corrosion.
(5) The cracking behavior derived in this study is based on some assumption mentioned in this study such as constant concrete cover parameters. In order to apply the outcome of this study to a general case of structure it is necessary to consider effects of other parameters. The outcome of this study may be useful for the maintenance process of an existing structure. That is, due to the difference of the rebar spacing, the internal damage situation may be different. So, the internal damage cannot adequately evaluate if the investigation is only based on the surface condition as being done in several current maintenance processes.

References

1) Andrade, C., Alonso, C. and Molina, F. J.: Cover cracking as a function of bar corrosion: Part I-Experimental test. *Materials and Structures,* Vol. 26, pp. 453-464,1993.
2) Oh, B.H., Kim, K.H. and Jang, B.S.: Critical corrosion amount to cause cracking of reinforced concrete structures, *ACI Material Journal,* Vol. 106 (4), pp.333-339, 2009.
3) Tsutsumi, T., Matsushima M. and Murakami, Y., Seki, H.: Study on crack models caused by pressure due to corrosion products, *Doboku Gakkai Ronbunshuu*, Vol. 30(2), pp. 159-166, 1996 (in Japanese).
4) Toongoenthong, K. and Maekawa, K.: Simulation of coupled corrosive product formation, migration into crack and propagation in reinforced sections. Journal of Advanced Concrete Technology 2005;3 (2):253-265.
5) Tran, K.K., Nakamura, H., Kawamura and K., Kunieda, M : Analysis of crack propagation due to rebar corrosion using RBSM, *Journal of Cement And Concrete Composites*, DOI:10.1016/j.cemconcomp.2011.06.001, 2011.
6) Murakami, Y., Oshita, H., Suzuki, S. and Tsutsumi, T.: Influence of stirrups and anchorage performance on residual strength of corroded RC beam, *Doboku Gakkai Ronbunshuu E,* Vol. 64(4), pp. 631-649, 2008 (in Japanese).
7) Ahmed, SFU., Maalej, M. and Mihashi, H.. Cover cracking of reinforced concrete beams due to corrosion of steel. *ACI Mater. J.*, Vol. 1042, pp. 153-161, 2007.
8) Kawai, T.: New element models in discrete structural analysis, *Journal of the Society of Naval Architects of Japan*, Vol. 141, pp. 187-193, 1977.
9) Bolander, J. E. and Saito, S.: Fracture analysis using spring network models with random geometry, *Engineering Fracture Mechanics*, Vol. 61, pp. 569-591, 1998.
10) Ueda, M., Kei, T. and Taniguchi, H.: Discrete limit analysis of reinforced concrete structures by RBSM, *Proceedings of JCI*, Vol. 10(3), pp. 335-338, 1988. (in Japanese).
11) Yashiro, R., Ishikawa, Y., Nakamura, H. and Tanabe, T.: Development of crack propagation analysis by RBSM considering mass transfer, *Proceeding of JCI meeting*, Japan Concrete Institute Vol. 25 (1), pp. 467-472,2003. (in Japanese).
12) Nagai, K., Sato, Y. and Ueda, T.: Mesoscopic simulation of failure of mortar and concrete by 2D RBSM, *Journal Of Advanced Concrete Technology*. Vol. 2(3), pp. 359-374, 2004.
13) Yamamoto Y., Nakamura H., Kuroda I. and Furuya N.: Analysis of compression failure of concrete by three dimensional Rigid Body Spring Model. *Doboku Gakkai Ronbunshuu,* Vol. 64(4), pp. 612-630, 2008 (in Japanese).
14) Nakamura, H. and Higai, T.: Compressive fracture energy and fracture zone length of concrete, modeling of inelastic behavior of RC structures under seismic loads, *American Society of Civil Engineers*, 627 V-44, pp. 471-487, 2001.
15) Saito, S.: Fracture analyses of structural concrete using spring network with random geometry. *Doctoral thesis*. Kyushu University 1999.
16) Tran, K K., Nakamura, H., Kunieda, M. and Ueda, N.: Three dimensional behavior of concrete cracking due to rebar corrosion, *Procedia Engineering,* Vol.(14), pp. 419-426, 2011.
17) Lundgren, K.: Modeling the effect of corrosion on bond in reinforced concrete, *Magazine of Concrete Research*, Vol. 54(3), pp. 165-173, 2002.
18) Yuan, Y. and Ji, Y.: Modeling corroded section configuration of steel bar in concrete structure. *Construction and Building Materials*; Vol. 23(6), pp. 2461-2466, 2009.
19) Kawamura, K., Tran, K.K., Nakamura, H. and Kunieda, M.: Surface crack propagation behavior against the surface deformation and inside cracks due to rebar corrosion, *Proceeding of JCI meeting*, Japan Concrete Institute Vol. 32 (1), pp. 1007-1012, 2010. (in Japanese).